AIP Journal of Applied Physics

Improvement of optical quality of semipolar (11$\bar{2}$2) GaN on m-plane sapphire by in-situ epitaxial lateral overgrowth

Morteza Monavarian, Natalia Izyumskaya, Marcus Müller, Sebastian Metzner, Peter Veit, Nuri Can, Saikat Das, Ümit Özgür, Frank Bertram, Jürgen Christen, Hadis Morkoç, and Vitaliy Avrutin

Citation: Journal of Applied Physics **119**, 145303 (2016); doi: 10.1063/1.4945770
View online: http://dx.doi.org/10.1063/1.4945770
View Table of Contents: http://scitation.aip.org/content/aip/journal/jap/119/14?ver=pdfcov
Published by the AIP Publishing

Articles you may be interested in
Efficient blocking of planar defects by prismatic stacking faults in semipolar (11 2 ¯ 2) -GaN layers on m-sapphire by epitaxial lateral overgrowth
Appl. Phys. Lett. **98**, 121916 (2011); 10.1063/1.3571455

Microstructural, optical, and electrical characterization of semipolar (11 2 ¯ 2) gallium nitride grown by epitaxial lateral overgrowth
J. Appl. Phys. **108**, 083521 (2010); 10.1063/1.3498813

Improved semipolar (11 2 ¯ 2) GaN quality using asymmetric lateral epitaxy
Appl. Phys. Lett. **94**, 191903 (2009); 10.1063/1.3134489

A -plane GaN epitaxial lateral overgrowth structures: Growth domains, morphological defects, and impurity incorporation directly imaged by cathodoluminescence microscopy
Appl. Phys. Lett. **92**, 212111 (2008); 10.1063/1.2920846

Improvement of microstructural and optical properties of GaN layer on sapphire by nanoscale lateral epitaxial overgrowth
Appl. Phys. Lett. **88**, 211908 (2006); 10.1063/1.2207487

Reuse of AIP Publishing content is subject to the terms at: https://publishing.aip.org/authors/rights-and-permissions. Download to IP: 128.172.168.211 On: Sun, 10 Apr 2016 17:03:26

JOURNAL OF APPLIED PHYSICS 119, 145303 (2016)

Improvement of optical quality of semipolar $(11\bar{2}2)$ GaN on *m*-plane sapphire by *in-situ* epitaxial lateral overgrowth

Morteza Monavarian,[1,a)] Natalia Izyumskaya,[1] Marcus Müller,[2] Sebastian Metzner,[2] Peter Veit,[2] Nuri Can,[1,3] Saikat Das,[1] Ümit Özgür,[1] Frank Bertram,[2] Jürgen Christen,[2] Hadis Morkoç,[1] and Vitaliy Avrutin[1]
[1]Department of Electrical and Computer Engineering, Virginia Commonwealth University, Richmond, Virginia 23284, USA
[2]Institute of Experimental Physics, Otto-von-Guericke-University Magdeburg, D-39106 Magdeburg, Germany
[3]Department of Physics, Balikesir University, Balikesir 10145, Turkey

(Received 19 November 2015; accepted 28 March 2016; published online 8 April 2016)

Among the major obstacles for development of non-polar and semipolar GaN structures on foreign substrates are stacking faults which deteriorate the structural and optical quality of the material. In this work, an *in-situ* SiN_x nano-network has been employed to achieve high quality heteroepitaxial semipolar $(11\bar{2}2)$ GaN on m-plane sapphire with reduced stacking fault density. This approach involves *in-situ* deposition of a porous SiN_x interlayer on GaN that serves as a nano-mask for the subsequent growth, which starts in the nanometer-sized pores (window regions) and then progresses laterally as well, as in the case of conventional epitaxial lateral overgrowth (ELO). The inserted SiN_x nano-mask effectively prevents the propagation of defects, such as dislocations and stacking faults, in the growth direction and thus reduces their density in the overgrown layers. The resulting semipolar $(11\bar{2}2)$ GaN layers exhibit relatively smooth surface morphology and improved optical properties (PL intensity enhanced by a factor of 5 and carrier lifetimes by 35% to 85% compared to the reference semipolar $(11\bar{2}2)$ GaN layer) which approach to those of the *c*-plane *in-situ* nano-ELO GaN reference and, therefore, holds promise for light emitting and detecting devices. © *2016 AIP Publishing LLC*. [http://dx.doi.org/10.1063/1.4945770]

I. INTRODUCTION

GaN layers of semipolar and nonpolar orientations have gained a great deal of attention owing to the suppression or reduction of spontaneous and piezoelectric polarization induced-quantum confined Stark effect (QCSE).[1–4] The ability to achieve heteroepitaxial semipolar $(11\bar{2}2)$ GaN having substantially reduced polarization on relatively inexpensive planar *m*-plane sapphire substrates[5,6] makes this semipolar orientation attractive for efficient and relatively cost-effective light emitting devices. Moreover, the interest in the $(11\bar{2}2)$ orientation is additionally fueled by theoretical works[7–9] predicting enhanced In incorporation efficiency supported by recent experimental reports,[10,11] which makes $(11\bar{2}2)$ structures particularly attractive for green light emitters. Despite the promises for future generations of long wavelength emitters based on semipolar $(11\bar{2}2)$, heteroepitaxy of this orientation of GaN on *m*-plane sapphire suffers from high density of extended defects, such as stacking faults (SFs)[12] and threading dislocations (TDs), resulting in low structural and optical quality.

Defect reduction methods such as epitaxial lateral overgrowth (ELO), inclusive of both *in-situ*[13–15] and *ex-situ*[16,17] varieties, which have been successfully used for *c*-plane GaN heterostuctures, are gaining popularity to improve optical and structural quality of semipolar structures intended for device applications. Up to now, the most common approach to improve the quality of $(11\bar{2}2)$ GaN is the growth on patterned sapphire[18–25] or Si[26] substrates. Although considerable progress was achieved in this field, the pattering process involves standard lithography, wet or reactive ion dry etching, and SiO_2 mask deposition, which is costly and time-consuming. On the other hand, the *in-situ* ELO method, also referred to as "nano-ELO," relies on *in-situ* deposition of thin porous SiN_x which acts as a mask and blocks extended defects.[13–15,27] This method is of great interest, because it does not require special preparation of substrates and potentially reduces the production cost. Today *in-situ* nano-ELO growth of *c*-plane oriented GaN templates on sapphire and Si is widely used in LED industry. This approach has been demonstrated to be effective in case of polar *c*-plane,[13–15,27] and nonpolar *a*-plane,[28,29] while the reports on defect reduction for the $(11\bar{2}2)$ orientation with this method are rare.[25,30–32]

Previously, we have reported on the improvement of optical and structural quality of semipolar $(11\bar{2}2)$ GaN layers by means of inserting nano-porous SiN_x interlayers.[33] In this work, we have further demonstrated optimization of the *in-situ* nano-ELO technique with the use of SiN_x interlayers deposited at higher temperatures in order to provide relatively smooth surface morphology required for device applications while offering improved optical quality.

II. EXPERIMENTAL PROCEDURE

The $(11\bar{2}2)$-oriented semipolar GaN layers used in experiments were grown on *m*-plane sapphire substrates in a vertical metal-organic chemical vapor deposition (MOCVD) system

a)Author to whom correspondence should be addressed. Electronic mail: monavarianm@vcu.edu

 © 2016 AIP Publishing LLC

Reuse of AIP Publishing content is subject to the terms at: https://publishing.aip.org/authors/rights-and-permissions. Download to IP: 128.172.168.211 On: Sun, 10 Apr 2016 17:03:26

with trimethylgallium (TMGa), trimethylaluminum (TMAl), and ammonia (NH_3) as the Ga, Al, and N precursors, respectively. SiH_4 gas was used for both Si-doping of the GaN layers and *in-situ* deposition of porous SiN_x interlayers. The growth progress was as follows: First, a thin (∼20 nm) AlN nucleation layer was deposited on the substrate at a substrate temperature of 500 °C followed by a ∼1–μm-thick GaN layer grown at 30 Torr and 1060 °C, which produces $(11\bar{2}2)$ orientation and ensures good surface morphology. Then, a ∼2.5–μm-thick GaN layer was grown at 200 Torr and 1040 °C to improve the optical quality. For the subsequent nano-ELO, the growth was interrupted to deposit a very thin porous SiN_x layer in a flow of SiH_4 and ammonia at a substrate temperature of 1040 °C and a reactor pressure of 200 Torr. A GaN seed layer was then grown for 20 min at the same pressure and temperature (Figure 1). Compared to our previous work,[33] the SiN_x interlayer was deposited at an elevated substrate temperature, which resulted in lower pore density in the SiN_x interlayers for a given deposition time. In our experiments, we varied the SiN_x deposition time from 1 to 3 min, keeping all other conditions the same. For the same deposition temperature, the longer the SiN_x deposition time is, the lower the pore density will be in the nano-mesh. Thus, for this set of experiments, depending on the SiN_x deposition time, different porosity of the SiN_x layers and, consequently, various densities of GaN islands were obtained, as illustrated schematically in Figures 1(a)–1(d). Finally, the GaN layers were overgrown at 200 Torr and 1040 °C and doped with Si to $\sim 2 \times 10^{18}\,cm^{-3}$ at 200 Torr reactor pressure to achieve the highest optical quality.

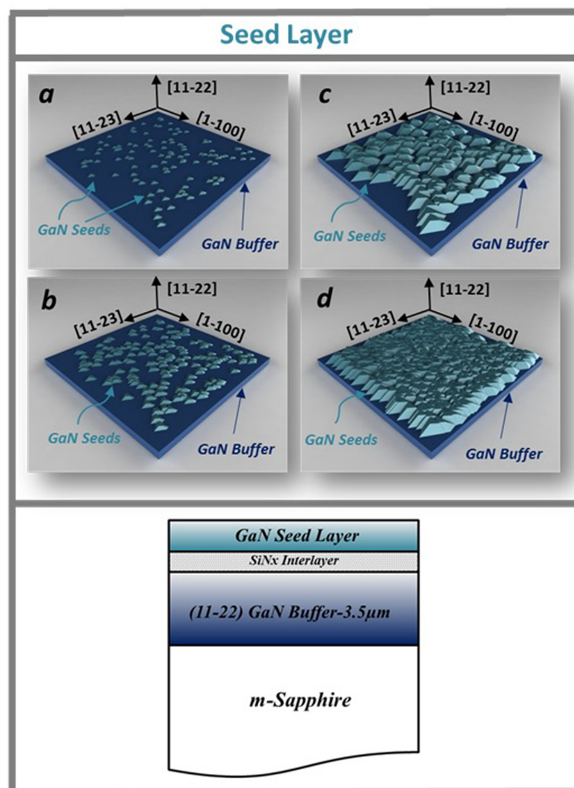

FIG. 1. Schematic drawing of the seed layer stage in the nano-ELO process, the density of nucleation islands increases (SiN_x deposition time decreases) from (a) to (d).

The total thickness of the GaN stack is 11.5 μm for all the samples. In this study, we used two reference samples. One is a *c*-plane GaN film which has been grown with the same *in-situ* nano-ELO technique on *c*-sapphire.[13] The second reference sample is a semipolar $(11\bar{2}2)$ GaN film grown on *m*-sapphire but without the SiN_x interlayer (referred to as the $(11\bar{2}2)$ GaN template). To provide a fair comparison of semipolar nano-ELO structures, the total thickness of the reference films was chosen to be similar.

Scanning electron microscopy (SEM) and atomic forced microscopy (AFM) were used to examine surface morphology. Optical properties of the layers were evaluated using steady state and time-resolved photoluminescence (PL). The steady-state PL measurements were performed using HeCd laser excitation ($\lambda = 325$ nm) for which the samples were mounted on a closed-cycle He-cooled cryostat for low temperature measurements. For the time-resolved PL (TRPL) measurements, a frequency-tripled pulsed Ti-sapphire laser (265 nm excitation) with a pulse-width of 150 fs and an excitation spot diameter of ∼50 μm and a Hamamatsu streak camera with 25 ps resolution were utilized. Cross-sectional scanning transmission electron microscopy (STEM) was utilized to evaluate the role of SiN_x interlayer in blocking the extended defects. The STEM analyses were performed in a scanning transmission electron microscope FEI (S)TEM Tecnai F20 equipped with a bright-field annular detector (BF) by the Gatan company. The sample was prepared in cross-section by mechanical wedge polishing combined with Ar+ion milling. Detailed information about the experimental setup and sample preparation can be found elsewhere.[34,35]

III. RESULTS AND DISCUSSION

To study the initial stage of the overgrowth on the SiN_x nano-mesh (Figure 1), the growth was stopped after 20 min of GaN on SiN_x and the samples were unloaded for surface morphology investigation under an optical microscope and SEM. The samples were then loaded back into the MOVCD chamber and the growth was resumed. Figures 2(a)–2(c) compare the surface morphology of the semipolar GaN samples overgrown for 20 min on the templates with different SiN_x deposition times. To reiterate, the porosity of the SiN_x layer is dependent on the deposition time: the shorter is the SiNx deposition time, the higher is the pore density in the nano-mesh, and GaN nucleates on the sites corresponding to the pores in SiN_x layer. Therefore, the density of nucleated GaN islands represents the porosity of the SiN_x nano-porous mask. The GaN layer on the 1-min SiN_x nano-mesh (Figure 2(a)) is fully coalesced after 20 min of growth (similar to case d in Figure 1), since the pore density, and consequently the density of GaN nuclei, is the highest in this case. The GaN layer on the 1.5-min SiN_x (Figure 2(b)) is partially coalesced (similar to case c in Figure 1), and the surface of the sample with 3-min SiN_x (Figure 2(c)) is covered with GaN islands that were nucleated in the pores with relatively low nucleation density (similar to the case b in Figure 1). Figure 2(d) shows an SEM image of the GaN islands on the template surface.

Figure 3 shows optical microscope images of the final surfaces of the 11.5 μm-thick nano-ELO samples. One can

Reuse of AIP Publishing content is subject to the terms at: https://publishing.aip.org/authors/rights-and-permissions. Download to IP: 128.172.168.211 On: Sun, 10 Apr 2016 17:03:26

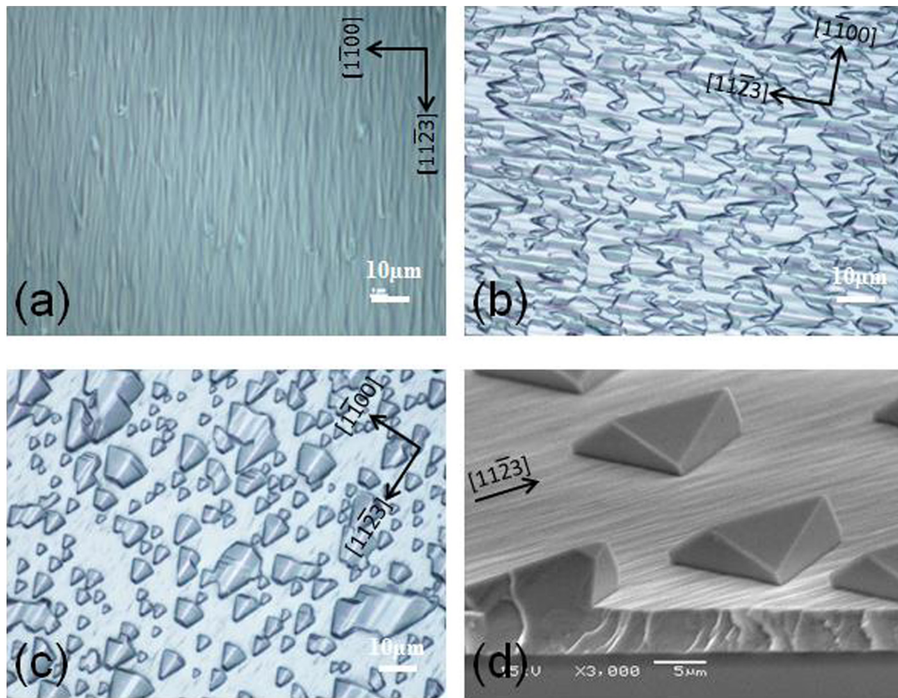

FIG. 2. Optical microscopy images of $(11\bar{2}2)$ GaN layer surface after 20 min of GaN growth on (a) 1-min, (b) 1.5-min, and (c) 3-min SiN_x interlayers. (d) Inclined view SEM image of semi-polar $(11\bar{2}2)$ GaN seeds on porous SiNx interlayer.

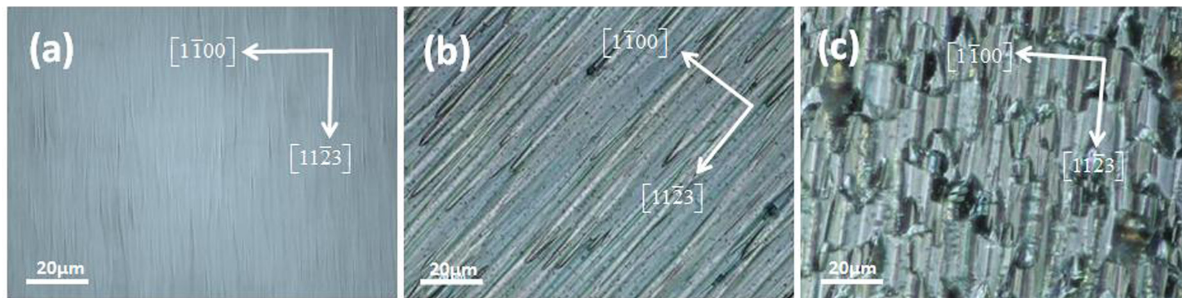

FIG. 3. Optical microscopy images of the final surface morphologies of *in-situ* nano-ELO $(11\bar{2}2)$ GaN layers grown with SiN_x interlayers deposited for (a) 1.0, (b) 1.5, and (c) 3.0 min.

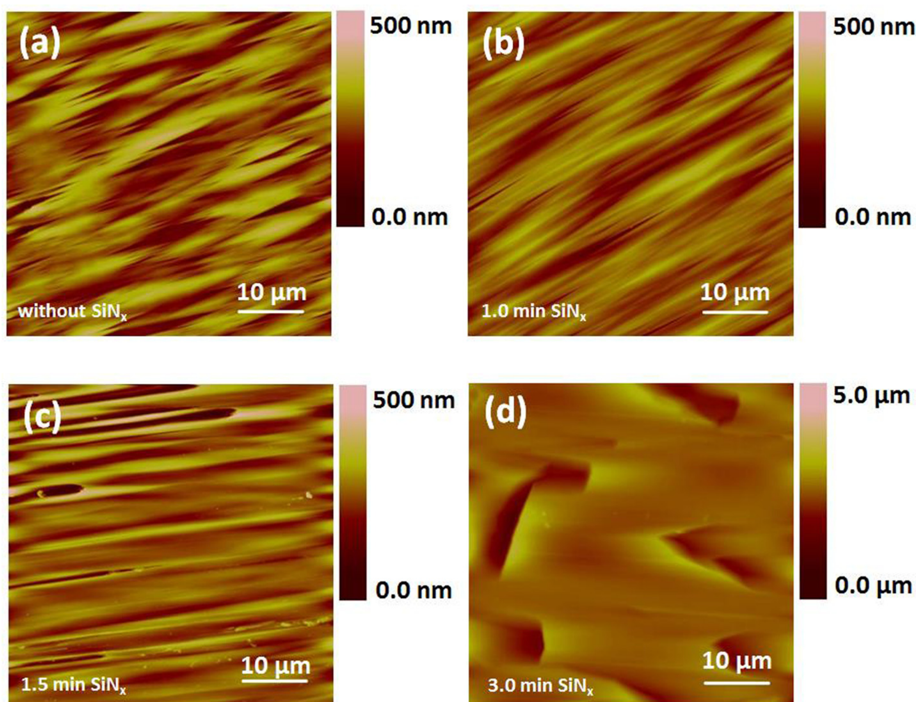

FIG. 4. AFM images of the semipolar $(11\bar{2}2)$ GaN layers grown on m-sapphire using porous SiNx interlayer with (a) 0.0 min (reference), (b) 1.0 min, (c) 1.5 min, and (d) 3.0 min deposition times. Note that the vertical scales are 500 nm except for (d) which is 5.0 μm.

Reuse of AIP Publishing content is subject to the terms at: https://publishing.aip.org/authors/rights-and-permissions. Download to IP: 128.172.168.211 On: Sun, 10 Apr 2016 17:03:26

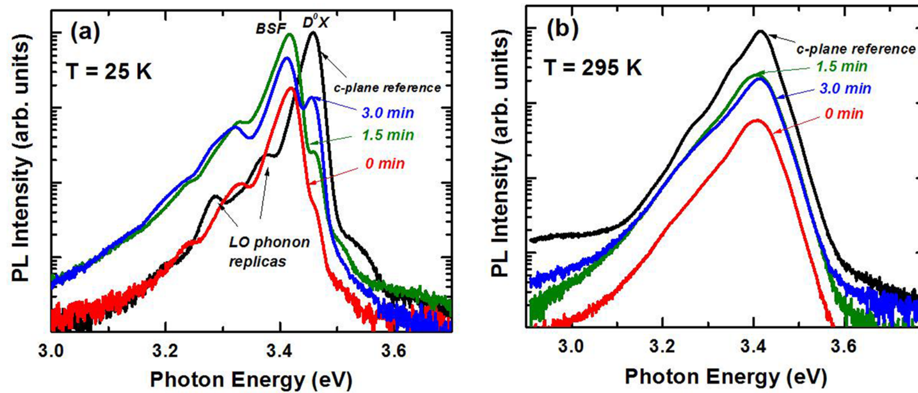

FIG. 5. (a) Low-temperature (25 K) and (b) room-temperature PL spectra for *in-situ* nano-ELO $(11\bar{2}2)$ GaN structures with SiN_x interlayers deposited for 1.5 min and 3 min in comparison with spectra for $(11\bar{2}2)$ GaN/*m*-sapphire template without SiN_x interlayer and *c*-plane nano-ELO GaN film.

see that the samples with 1- and 1.5-min SiN_x interlayers have fully coalesced surface with arrow-like features elongated in the $[11\bar{2}3]$ direction of GaN (Figures 3(a) and 3(b)), which is a characteristic of $(11\bar{2}2)$ GaN layer surface.[36] The sample with 3-min SiN_x interlayer, however, suffers from holes and rough V-shaped features (Figure 3(c)). AFM images of the samples with 1.0-, 1.5-, 3.0-min SiN_x interlayers and the reference $(11\bar{2}2)$ GaN template are displayed in Figure 4. The root-mean-square (rms) values measured on $50\,\mu m \times 50\,\mu m$ areas are 53, 34, 50, and 251 nm for layers having 0, 1.0, 1.5, and 3.0 min SiN_x deposition times, respectively. Thus, the sample with the shortest SiNx deposition time shows the best surface morphology.

Figure 5(a) shows low-temperature (25 K) PL spectra of the samples under study. One can see that the spectrum for the $(11\bar{2}2)$ GaN template grown without the SiN_x interlayer is dominated by a peak centered around 3.425 eV (362 nm) related to basal plane stacking faults (BSFs),[37,38] while donor-bound exciton (D^0X) emission is seen only as a weak shoulder at 3.464 eV (358 nm). It should be mentioned that the BSF density in the layer can be correlated to the ratio of D^0X-to-BSF related intensities rather than to the BSF intensity by itself, as the BSF emission intensity can also be suppressed due to higher density of nonradiative centers, which include point defects and dislocations. The low value of the ratio of D^0X-to-BSF emission intensities is indicative of a large contribution from BSFs, thus suggesting their high density in the reference sample. It should be noted that the overall PL intensity, to the large extent, is limited by the density of dislocations (which are nonradiative defects), rather than stacking faults (which are optically active). For the sample grown with 1.5-min SiN_x, the intensity of both BSF-related and DX low-temperature PL lines as well as room-temperature PL intensity (Figure 5(a)) considerably increase compared to the reference sample grown without SiN_x, although the D^0X-to-BSF intensity ratio improved only slightly compared to the reference sample. This implies that the 1.5-min SiN_x nanomesh effectively blocks dislocations rather than BSFs. Employment of the 3-min SiN_x interlayer improves the D^0X-to-BSF intensity ratio, thus suggesting the reduction in the BSF density in this sample. However, as apparent from the low-temperature PL spectrum (Figure 5(a)), the BSF density is still high.

Figure 5(b) compares the room-temperature PL spectra obtained from the *in-situ* nano-ELO $(11\bar{2}2)$ GaN films with those from the $(11\bar{2}2)$ GaN reference sample without any SiN_x interlayer and the *c*-plane nano-ELO reference sample. One can see that the introduction of the SiN_x interlayer considerably improves the room-temperature PL intensity; the emission intensity from the sample with 1.5-min interlayer is only 3.8 times lower than that for the *c*-plane nano-ELO layer, while the PL intensity from the $(11\bar{2}2)$ GaN reference sample without the SiN_x interlayer is approximately 20 times lower, suggesting that a PL intensity improvement by more than 5 times is obtained by applying the nano-ELO technique. It should be mentioned that the PL intensity is improved by a factor of 2 (on average) compared to the layers obtained in a previous study[33] which were grown at a lower SiN_x deposition temperature (by 15 °C). We can explain this improvement by the fact that the increase in SiN_x deposition temperature results in less porous nano-mesh, which more effectively blocks the nonradiative defects. In addition, the surface morphology is significantly improved compared to our structures reported earlier.[33]

To investigate the effect of *in-situ* nano-ELO on carrier dynamics, we have performed time-resolved PL (TRPL) measurements. Figure 6 depicts PL transients for the $(11\bar{2}2)$ GaN samples with SiN_x interlayers measured with an excitation power density of $240\,W/cm^2$ at room temperature. As seen from the figure, the transients exhibit single exponential decay. We have found that, while $(11\bar{2}2)$ GaN layers grown without SiN_x interlayers but with identical total thickness exhibit a fast decay of about 0.15 ns, the PL decay times for the nano-ELO semipolar samples are longer by 35% to 85% (with 0.20 and 0.27 ns for the samples with 1.5- and 3.0-min SiN_x interlayers, respectively), although still shorter than that for the polar *c*-plane reference layer (0.66 ns). Thus, the TRPL data also indicate that the nano-ELO technique results in considerable improvement of the optical quality of semipolar material. Moreover, the increase in carrier lifetime as a function of SiN_x deposition time (demonstrated in the inset of Figure 6) is consistent with the reported data on the optimization of nano-ELO technique for the case of *c*-plane GaN grown on *c*-sapphire.[13]

The reduction in BSF density due to the SiN_x interlayer, as concluded from the enhancement of the D^0X emission with respect to BSF-related PL line (see Figure 5(a)), is also supported by STEM data. Figure 7 shows a cross-sectional bright field STEM image of a semipolar nano-ELO structure grown at a lower SiN_x deposition temperature of 1025 °C (more details can be found elsewhere[33]). A high density of basal plane stacking faults running at an angle of 58.4° with

Reuse of AIP Publishing content is subject to the terms at: https://publishing.aip.org/authors/rights-and-permissions. Download to IP: 128.172.168.211 On: Sun, 10 Apr 2016 17:03:26

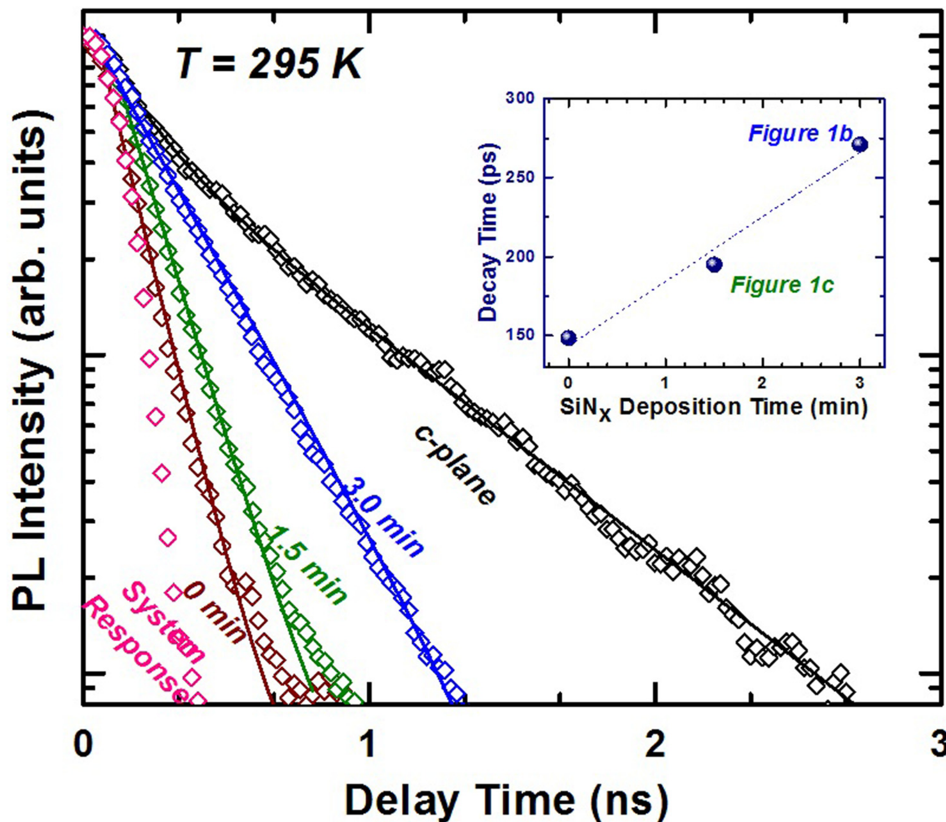

FIG. 6. Time-resolved PL intensities for *in-situ* nano-ELO $(11\bar{2}2)$ GaN with SiN_x interlayers deposited for 1.5 min and 3 min compared to reference layer without interlayer. The data for the *c*-plane GaN film prepared by the *in situ* nano-ELO technique are also shown for comparison. Solid lines are exponential fits. The inset demonstrates correlation between room temperature PL decay time and SiN_x deposition time, and consequently, seed morphology.

respect to semi-polar surface can be clearly seen in darker contrast in the bottom GaN layer. Importantly, it is clearly seen that the BSFs are locally blocked fairly efficiently at the SiN_x interlayer resulting in a significantly reduced BSF density in the upper semi-polar GaN layer. The improvement in BSF density for the nano-ELO layer (above the nano-mesh) compared to the semipolar template (below the nano-mesh) correlates with the improvement in the D^0X-to-BSF intensity ratio for the nano-ELO compared to the reference semipolar layer. In the low-temperature PL spectrum exhibited by this sample (not shown), the D^0X-to-BSF intensity ratio was improved by a factor of 4 compared to the reference $(11\bar{2}2)$ layer without nano-mesh.

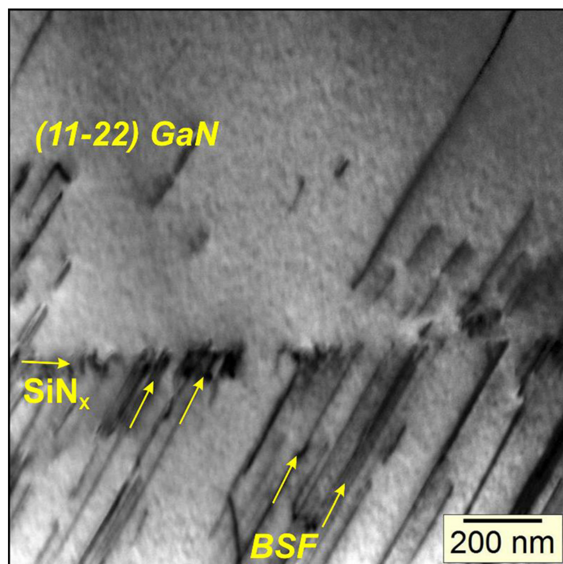

FIG. 7. Cross-sectional STEM image in bright field contrast of *in-situ* nano-ELO $(11\bar{2}2)$-oriented semipolar GaN layer grown on 2-min SiN_x nano-mesh deposited at 1025 °C.

The data obtained indicate that the insertion of the SiN_x interlayer improves the surface morphology as well as optical properties of the overgrown $(11\bar{2}2)$ GaN layer. However, there is a trade-off between surface morphology and optical quality; the increase in SiN_x deposition time improves the optical quality with the cost of increase in surface roughness. More extensive studies of the semipolar nano-ELO structures by means of cross sectional STEM in combination with spectrally and spatially resolved cathodoluminescence are in progress, and the results will be reported elsewhere.

IV. CONCLUSIONS

In summary, employment of the *in-situ* nano-ELO technique leads to semipolar $(11\bar{2}2)$ GaN layers with relatively smooth surface morphology and optical properties (PL intensity and carrier lifetimes) approaching to those of the *c*-plane GaN. An enhancement in the room-temperature photoluminescence intensity by a factor of 5 has been attained for layers with SiN_x nanomesh compared to the layer with identical total thickness but without the SiN_x interlayer. The recombination lifetime was found to increase from 150 to 270 ps with the deposition time of the SiN_x nanomesh when a 3 min SiN_x interlayer was used.

ACKNOWLEDGMENTS

The work at VCU was funded by a Materials World Network grant from the National Science Foundation (DMR-1210282) under the direction of C. Ying. The work at

Reuse of AIP Publishing content is subject to the terms at: https://publishing.aip.org/authors/rights-and-permissions. Download to IP: 128.172.168.211 On: Sun, 10 Apr 2016 17:03:26

Magdeburg University is funded by the German Research Foundation, DFG, in the frame of the research unit FOR 957 "PolarCoN." Nuri Can acknowledges the Ph.D. grant support from the scientific and technological research council of Turkey (TUBITAK). The authors would like to thank Mr. Shopan Hafiz for his help in regard to the preparation of time-resolved PL setup and Mr. Farid Ghanbari for helping us with the schematics drawings.

[1]V. Fiorentini, F. Bernardini, F. Della Sala, A. Di Carlo, and P. Lugli, Phys. Rev. B **60**, 8849 (1999).
[2]T. Deguchi, K. Sekiguchi, A. Nakamura, T. Sota, R. Matsuo, S. Chichibu, and S. Nakamura, Jpn. J. Appl. Phys., Part 2 **38**, L914 (1999).
[3]R. Langer, J. Simon, V. Ortiz, N. T. Pelekanos, A. Barski, R. André, and M. Godlewski, Appl. Phys. Lett. **74**, 3827 (1999).
[4]M. Zamfirescu, B. Gil, N. Grandjean, G. Malpuech, A. Kavokin, P. Bigenwald, and J. Massies, Phys. Rev. B **64**, 121304 (2001).
[5]P. Vennéguès, T. Zhu, D. Martin, and N. Grandjean, J. Appl. Phys. **108**, 113521 (2010).
[6]T. J. Baker, B. A. Haskell, F. Wu, J. S. Speck, and S. Nakamura, Jpn. J. Appl. Phys., Part 2 **45**, L154 (2006).
[7]M. V. Durnev, A. V. Omelchenko, E. V. Yakovlev, I. Y. Evstratov, and S. Y. Karpov, Appl. Phys. Lett. **97**, 051904 (2010).
[8]J. E. Northrup, Appl. Phys. Lett. **95**, 133107 (2009).
[9]A. Strittmatter, J. E. Northrup, N. M. Johnson, M. V. Kisin, P. Spiberg, H. El-Ghoroury, A. Usikov, and A. Syrkin, Phys. Status Solidi B **248**, 561 (2011).
[10]Y. Zhao, Q. Yan, C.-Y. Huang, S.-C. Huang, P. S. Hsu, S. Tanaka, C.-C. Pan, Y. Kawaguchi, K. Fujito, C. G. V. de Walle, J. S. Speck, S. P. DenBaars, S. Nakamura, and D. Feezell, Appl. Phys. Lett. **100**, 201108 (2012).
[11]M. Monavarian, S. Metzner, N. Izyumskaya, S. Okur, F. Zhang, N. Can, S. Das, V. Avrutin, Ü. Özgür, F. Bertram, J. Christen, and H. Morkoç, Proc. SPIE **9363**, 93632P (2015).
[12]S. Okur, M. Monavarian, S. Das, N. Izyumskaya, F. Zhang, V. Avrutin, H. Morkoç, and Ü. Özgür, Proc. SPIE **9363**, 93632N (2015).
[13]J. Xie, Ü. Özgür, Y. Fu, X. Ni, H. Morkoç, C. K. Inoki, T. S. Kuan, J. V. Foreman, and H. O. Everitt, Appl. Phys. Lett. **90**, 041107 (2007).
[14]S. Haffouz, V. Kirilyuk, P. R. Hageman, L. Macht, J. L. Weyher, and P. K. Larsen, Appl. Phys. Lett. **79**, 2390 (2001).
[15]J. Hertkorn, F. Lipski, P. Brückner, T. Wunderer, S. B. Thapa, F. Scholz, A. Chuvilin, U. Kaiser, M. Beer, and J. Zweck, J. Cryst. Growth **310**, 4867 (2008).
[16]P. Vennéguès, Semicond. Sci. Technol. **27**, 024004 (2012).
[17]N. Kriouche, P. Vennéguès, M. Nemoz, G. Nataf, and P. De Mierry, J. Cryst. Growth **312**, 2625 (2010).
[18]P. Vennéguès, F. Tendille, and P. De Mierry, J. Phys. D: Appl. Phys. **48**, 325103 (2015).
[19]F. Tendille, M. Hugues, P. Vennéguès, M. Teisseire, and P. De Mierry, Semicond. Sci. Technol. **30**, 065001 (2015).
[20]H. Furuya, N. Okada, and K. Tadatomo, Phys. Status Solidi C **9**, 568 (2012).
[21]N. Okada, A. Kurisu, K. Murakami, and K. Tadatomo, Appl. Phys. Express **2**, 091001 (2009).
[22]Q. Sun, C. D. Yerino, B. Leung, J. Han, and M. E. Coltrin, J. Appl. Phys. **110**, 053517 (2011).
[23]F. Scholz, T. Meisch, M. Caliebe, S. Schörner, K. Thonke, L. Kirste, S. Bauer, S. Lazarev, and T. Baumbach, J. Cryst. Growth **405**, 97 (2014).
[24]D. V. Dinh, M. Akhter, S. Presa, G. Kozlowski, D. O'Mahony, P. P. Maaskant, F. Brunner, M. Caliebe, M. Weyers, F. Scholz, B. Corbett, and P. J. Parbrook, Phys. Status Solidi A **212**, 2196 (2015).
[25]M. Caliebe, T. Meisch, B. Neuschl, S. Bauer, J. Helbing, D. Beck, K. Thonke, M. Klein, D. Heinz, and F. Scholz, Phys. Status Solidi C **11**, 525 (2014).
[26]J. Bai, X. Yu, Y. Gong, Y. N. Hou, Y. Zhang, and T. Wang, Semicond. Sci. Technol. **30**, 065012 (2015).
[27]J. Xie, Y. Fu, X. Ni, S. Chevtchenko, and H. Morkoç, Appl. Phys. Lett. **89**, 152108 (2006).
[28]J. L. Hollander, M. J. Kappers, C. McAleese, and C. J. Humphreys, Appl. Phys. Lett. **92**, 101104 (2008).
[29]T. S. Ko, T. C. Wang, H. M. Huang, J. R. Chen, H. G. Chen, C. P. Chu, T. C. Lu, H. C. Kuo, and S. C. Wang, J. Cryst. Growth **310**, 4972 (2008).
[30]J. Jeong, J. Jang, J. Hwang, C. Jung, J. Kim, K. Lee, H. Lim, and O. Nam, J. Cryst. Growth **370**, 114 (2013).
[31]Y. A. R. Dasilva, M. P. Chauvat, P. Ruterana, L. Lahourcade, E. Monroy, and G. Nataf, J. Phys.: Condens. Matter **22**, 355802 (2010).
[32]M. Pristovsek, M. Frentrup, Y. Han, and C. J. Humphreys, Phys. Status Solidi B **253**, 61–66 (2016).
[33]M. Monavarian, S. Metzner, N. Izyumskaya, M. Müller, S. Okur, F. Zhang, N. Can, S. Das, V. Avrutin, Ü. Özgür, F. Bertram, J. Christen, and H. Morkoç, Proc. SPIE **9363**, 93632I (2015).
[34]M. Müller, G. Schmidt, S. Metzner, P. Veit, F. Bertram, R. A. R. Leute, D. Heinz, J. Wang, T. Meisch, F. Scholz, and J. Christen, Phys. Status Solidi B **253**, 112 (2016).
[35]G. Schmidt, M. Müller, P. Veit, F. Bertram, J. Christen, M. Glauser, J.-F. Carlin, G. Cosendey, R. Butté, and N. Grandjean, Appl. Phys. Lett. **105**, 032101 (2014).
[36]S. Ploch, J. Bum Park, J. Stellmach, T. Schwaner, M. Frentrup, T. Niermann, T. Wernicke, M. Pristovsek, M. Lehmann, and M. Kneissl, J. Cryst. Growth **331**, 25 (2011).
[37]R. Liu, A. Bell, F. A. Ponce, C. Q. Chen, J. W. Yang, and M. A. Khan, Appl. Phys. Lett. **86**, 021908 (2005).
[38]P. P. Paskov, R. Schifano, B. Monemar, T. Paskova, S. Figge, and D. Hommel, J. Appl. Phys. **98**, 093519 (2005).

Reuse of AIP Publishing content is subject to the terms at: https://publishing.aip.org/authors/rights-and-permissions. Download to IP: 128.172.168.211 On: Sun, 10 Apr 2016 17:03:26